Direct Observation of Deviations from Taylor's Frozen Hypothesis and Scaling Laws in Canonical Jet Flows

Sukesh Roy
Spectral Energies, LLC
Joseph Miller
Gemunu Gunaratne (gemunu@uh.edu)
University of Houston https://orcid.org/0000-0001-9638-9599

Article

Keywords: frozen, canonical, burst-mode, anisotropic

Posted Date: September 1st, 2020

DOI: https://doi.org/10.21203/rs.3.rs-63155/v1

Version of Record: A version of this preprint was published at Communications Physics on February 22nd, 2021. See the published version at https://doi.org/10.1038/s42005-021-00528-0.

Deviations from Taylor's Frozen Hypothesis and Scaling Laws in Inhomogeneous Jet Flows

Sukesh Roy,[1,*] Joseph D. Miller,[2] Gemunu H. Gunaratne[3,†]

[1]*Spectral Energies, LLC, Dayton, OH 45431*

[2] *Air Force Research Laboratory, Wright-Patterson Air Force Base, OH 45433*

[3]*Department of Physics, University of Houston, Houston, TX 77204**

(Dated: August 20, 2020)

* roy.sukesh@gmal.com, †gemunu@uh.edu

The legendary difficulties in studying turbulent flows stem, in part, from the lack of high-frequency, high-resolution measurements to interrogate small-scale structures and their rapid evolution. Our experiments, employing a burst-mode laser system, capture both spatially resolved velocity fields and their dynamics using high-resolution particle image velocimetry measurements at 100 kHz. We show directly that fluctuations of flow velocity in an axisymmetric jet flow are inhomogeneous and anisotropic. The velocity of the peak of the time-delayed cross correlation function $C(\mathbf{r}, \mathbf{r}'; \tau)$ is smaller than the convection velocity; thus Taylor's frozen hypothesis [Taylor GI, Proc. R. Soc. London, Ser A 164, 476 (1938)] fails to generalize for inhomogeneous jet flows, consistent with prior studies. Its peak decays exponentially in time. Second, the structure functions are found to be isotropic at small distances, but not at large distances. Extended self-similarity is found to hold [Benzi R et al., Physics Review E 48, R29 (1993)], but no inertial range is found where the *Kolmogorov* $\frac{2}{3}$*-law* [Kolmogorov AN, Dokl. Akad. Naud. SSSR 30, 299 (1941)] holds. Spectral-energy density of the jet flow, although anisotropic, is consistent with the *Kolmogorov-Obukhov* $\frac{5}{3}$*-law* [Obukhov AM, Izvestiya Akad. Nauk. SSSR 32, 19 (1941)] in the flow direction.

Time-averaged velocity fields of turbulent flows are studied as a function of the Reynold's number $Re = vL_s/\nu$, where v and L_s are characteristic flow velocity and length scale in the flow, and ν the kinematic viscosity [1, 2]. The flow transitions from laminar to turbulent as Re increases beyond a threshold. The dynamics of the consequent small-scale structures in turbulent flows are chaotic and are typically characterized through appropriate statistical objects such as cross correlation coefficients and structure functions [2]. Most theoretical developments are predicated on general considerations on energy transmission between scales [3–5]. Specifically, it is assumed that a hierarchy of eddies of different scales acts as intermediaries in energy transmission [6]. Eddies whose size is larger than the *Taylor microscale* $\lambda = \sqrt{10}L_s Re^{-1/2}$ transmit the entire energy to smaller scales; viscous dissipation is only active at scales smaller than λ [7]. The smallest scale of turbulent flow is the *Kolmogorov scale* $\eta = L_s Re^{-3/4}$, by which point viscosity has induced complete energy dissipation [3]. The derivation of observed facets of statistical objects requires an additional assumption that for sufficiently large Re, small-scale turbulence is isotropic and homogeneous [3]. This

assumption is justified by noting the reduction of inhomogeneity and anisotropy during the energy transfer between scales due to the chaotic nature of the flow [2]. Under these conditions dimensional analysis yields two celebrated results: (1) the "$\frac{2}{3}$-law," on the growth of structure functions and (2) the "$\frac{5}{3}$-law" on the decay in spectral-energy density [2, 3, 5]. Although these predictions have been experimentally verified in some configurations [8], anomalous scaling of higher order structure functions [9] and anisotropic effects [10–12] have been reported in others. Since these experiments lacked data with sufficiently high spatial resolution, the statistical analyses relied on *Taylor's frozen hypothesis*, that turbulent fluctuations propagate downstream with no change [7, 13, 14].

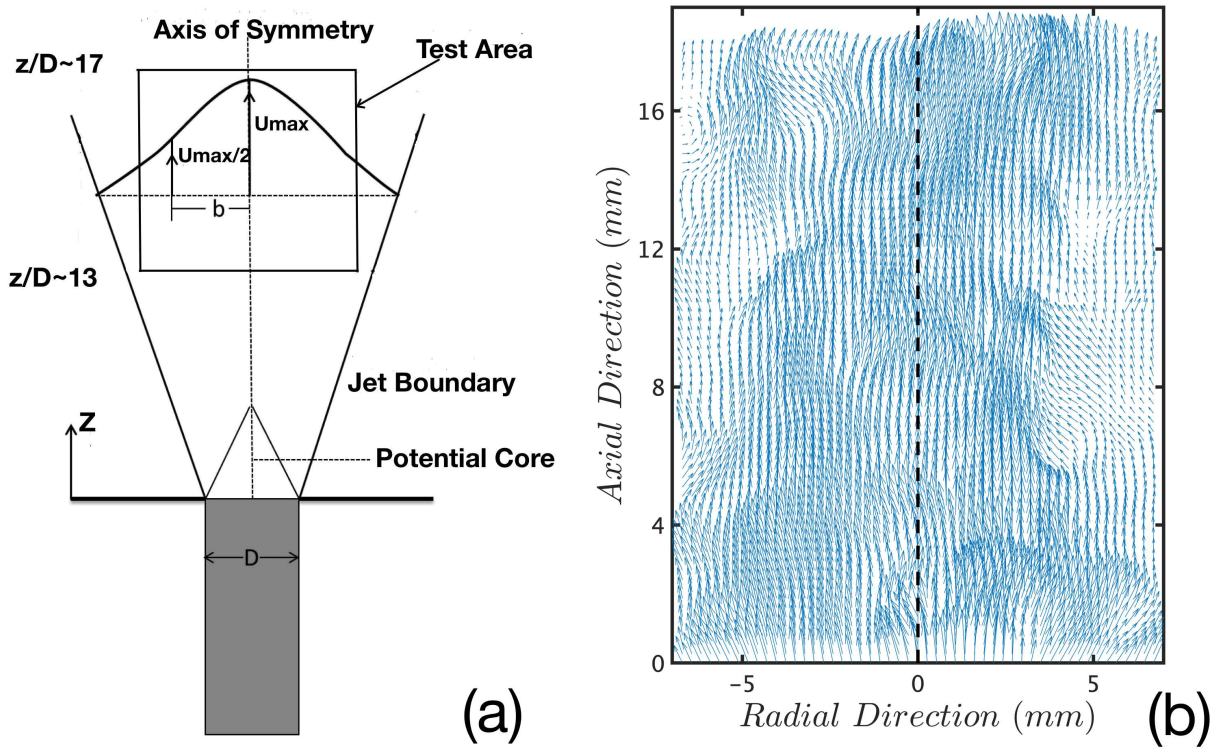

FIG. 1. (a) Axisymmetric jet flow is generated by N_2 gas ejected from cylinder of radius $D = 4.7$ mm. Rectangular region of size 13.4 $mm \times 17.7$ mm where velocity measurements were made was approximately $13D$ downstream of inlet. (b) Snapshot of velocity field for flow of $Re \approx 78,000$.

The critical technology that facilitated the resolution of the turbulent flow in both spatial and temporal domains was the development of a long-duration (100-ms), high-energy burst-mode laser capable of producing pairs of pulses at a rate of 5 kHz to 1 MHz [15, 16]. It permitted the performance of two-dimensional velocity measurements employing particle

image velocimetry (PIV) at a rate of 100 kHz and a resolution of flow features (both spatially and temporally) almost down to the Taylor micro-scale for $Re < 80,000$. For example, at 100 kHz in the present study, we acquired $\sim$ 8,500 velocity-field snapshots within the 100-ms duration. Turbulent jet flows of Re between 21,000 and 78,000 emanated from a cylindrical inlet of diameter $D = 4.7$ mm. As it moved downstream, the axisymmetric flow expanded (nearly) linearly. Velocity measurements at 100 kHz were made on a grid of 51×67 of lattice size 0.268 mm placed symmetrically in an axial plane approximately $13D$ downstream of the inlet, as shown in Figure 1(a). Figure 1(b) is a snapshot of the flow velocity field for $Re \approx 78,000$. The Taylor micro-scale and the Kolmogorov scale for the flow are 165 μm and 3 μm respectively. Statistical objects were computed through time averages, which were assumed to be reliable surrogates for ensemble averages [2]. Since the lattice size $\sim$ Taylor micro-scale, nearly the entire inertial scale could be examined.

The time average of the velocity field $\mathbf{v}(\mathbf{R};t)$ and its deviation from the mean are denoted $\bar{\mathbf{v}}(\mathbf{R})$ and $\mathbf{v}'(\mathbf{R};t)$ respectively, where $\mathbf{R}$ is measured from the center of the near-boundary. The axial and radial projections $\bar{v}_z(\mathbf{R})$ and $\bar{v}_r(\mathbf{R})$ are given by the Tollmien solution [17, 18] derived by expressing the Reynold's equation [1] in cylindrical polar coordinates (r, θ, z) and noting that for sufficiently large Re, the viscous stresses are insignificant compared to turbulent shear stresses. As shown in Supplementary Materials, the experimental velocity fields satisfy the Tollmien solution, which is neither isotropic nor homogeneous. It has generally been posited that even in such cases, small-scale turbulent flows are isotropic and homogeneous at sufficiently large Re [2]. However, more recent work has cautioned against the conjecture for inhomogeneous flows [19]. One advantage of the spatio-temporal jet-flow data obtained in the present study is that they can be used to perform a direct test of the symmetries of $\mathbf{v}'(\mathbf{R};t)$ down to the scale of the lattice (~ 0.27 mm) [16, 20]. The results for $v'_z(r,z;t)$ and $v'_r(r,z;t)$ can be summarized as follows. Their standard deviations decrease along the flow axis and are nearly constant in the radial direction except near the edge of the domain, where they decay. As shown in Supplementary Materials, the corresponding turbulent intensity $\mathcal{T} \equiv \sigma[v'_z]/\bar{v}_z$ [14] is nearly constant along the z axis and increases from ~ 0.1 to ~ 0.6 in the radial direction. The question we address is if and how Taylor's frozen hypothesis and scaling laws for structure functions and spectral energy densities are affected by the inhomogeneity and anisotropy of axisymmetric jet flows.

We implement a pre-processing step to eliminate recurrent features of the flow, whose

origins may lie in imperfections of the experimental set-up, acoustic reflections from laboratory walls, etc. Theoretical approaches consider only the remaining non-reccurent facets of a flow. The implementation, based on *robust mode analysis* [21], is outlined in Supplementary Materials. For jet flow at $Re \approx 78,000$, we find, and eliminate, one recurrent global mode of period 0.72 ms.

CROSS-CORRELATION COEFFICIENT

Incompressibility of the fluid, diffusion, as well as the presence of tube-like vortex structures [22, 23] induce correlations between velocity fluctuations at neighboring sites in turbulent flows. Among measures used for quantitative assessment are the time-delayed cross-correlation coefficient

$$C\left(\mathbf{R},\mathbf{R}';\tau\right)=\frac{\left\langle \mathbf{v}'(\mathbf{R};t)\cdot\mathbf{v}'(\mathbf{R}';t+\tau)\right\rangle_t}{\sigma\left[\mathbf{v}'(\mathbf{R})\right]\sigma\left[\mathbf{v}'(\mathbf{R}')\right]}, \tag{1}$$

and the analogous quantities $C_z(\mathbf{R},\mathbf{R}';\tau)$ and $C_r(\mathbf{R},\mathbf{R}';\tau)$ for the axial and radial velocity components. Here $\sigma\left[\mathbf{v}'(\mathbf{R})\right]$ is the standard deviation of the signal $\mathbf{v}'(\mathbf{R};t)$. Note that $C\left(\mathbf{R},\mathbf{R}';\tau=0\right)\to 1$ as $|\mathbf{R}'-\mathbf{R}|\to 0$. When Taylor's frozen hypothesis [7, 13, 14] is valid, $C\left(\mathbf{R},\mathbf{R}';\tau\right)=1$ for sufficiently nearby points $\mathbf{R}'$ downstream of $\mathbf{R}$ for $\tau=|\mathbf{R}'-\mathbf{R}|/\bar{v}_z$. Its validity for inhomogeneous flows has been debated [19, 24]. In the absence of a theoretical framework, spatio-temporal data is indispensable to establish, if and how the hypothesis is modified for inhomogeneous flows. Analyses outlined below were conducted on recordings from four 15 ms intervals (*i.e.,* 1500 snapshots) of the data; the error bars are standard deviations.

Figure 2 summarizes features of the cross-correlation coefficient with $\mathbf{R}=\mathbf{0}\equiv(0,0)$ for jet flows at $Re\approx 78,000$. The upper panel shows three snapshots of $C\left(\mathbf{0},\mathbf{R}';\tau\right)$, which is seen to contain a growing downstream-flowing peak. Denote the mean flow velocity at the n'th lattice site on the symmetry axis as $\bar{v}_z(n)$, which, as shown in Supplementary Materials, is a decreasing function of n. The time t_n for a signal at the origin to reach the n'th lattice site is bounded by $\sum_{m=1}^{n}\delta/\bar{v}_z(m)<t_n<\sum_{m=0}^{n-1}\delta/\bar{v}_z(m)$, where $\delta=0.268$ mm is the lattice size. The bounds are indistinguishable, and the line $(t_n,n\delta)$ is shown in red in Figure 2(b). The position of the peak, shown by blue symbols in Figure 2(b), flows at $\sim 80\%$

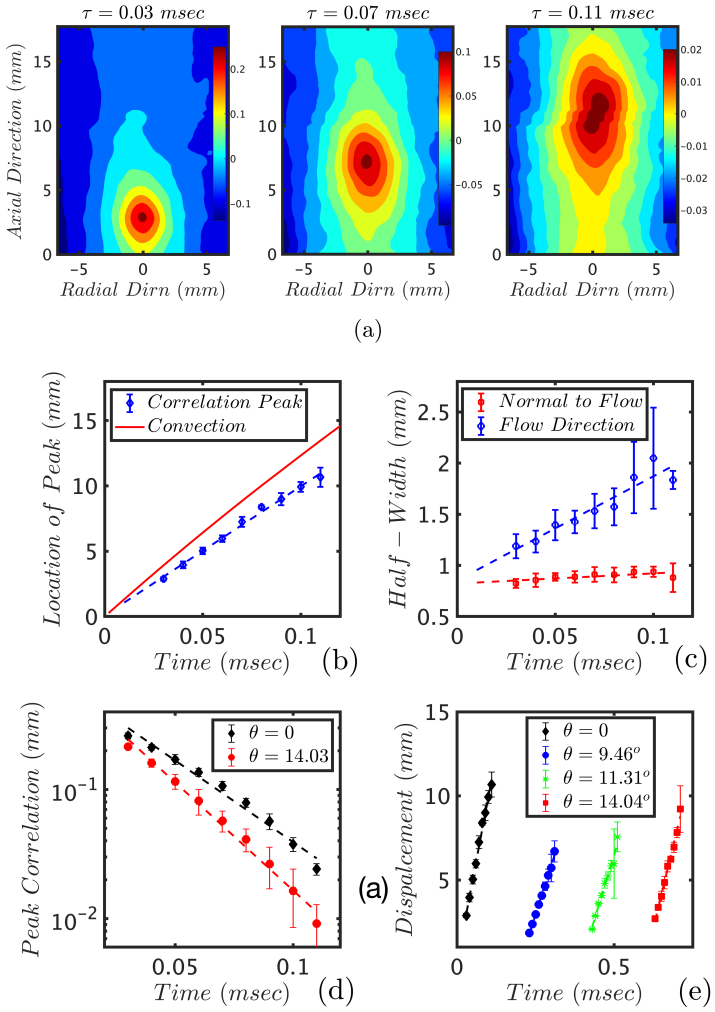

FIG. 2. (a) Three snapshots of the field $C(\mathbf{R}=\mathbf{0},\mathbf{R}';\tau)$, whose peak flows downstream and broadens in time. Distances are given in *mm* and the center of the near-boundary is chosen as the origin. (b) The downstream velocity of the peak is smaller than the convection velocity. (c) The width of the peak, both in the flow direction and normal to it, grows linearly in time. (d) The peak $P_z(\tau)$ (flow direction: $\theta = 0$) decays exponentially in time. (e) Velocity of the peak is nearly independent of the direction inside of a cone. The lines (shifted for clarity) show the peak locations as a function of time for the flow direction and for directions oriented $\theta = tan^{-1}(1/6)$, $tan^{-1}(1/5)$, and $tan^{-1}(1/4)$ from the flow axis. However, as seen in (d), the peak intensity decays faster as one moves away from the flow direction.

of this convection velocity, consistent with prior studies [25, 26]. (Deviations are found at off-axial sites as well, but with differing ratio of velocities.) The difference is most easily explained through Lagrangian flow; *i.e.,* description from a frame co-moving with the axial flow. As any velocity fluctuation diffuses to neighboring sites, where the flow-velocity is negative (since the velocity is highest on the symmetry axis), thus dragging the disturbance

backward. The deviation of the peak velocity from the convection velocity is thus due to the inhomogeneity in mean flow, as given by the Tollmien solution [17].

A second modification to Taylor's hypothesis, under which the peak intensity remains 1, is an exponential decay of the peak, see Figure 2(d). We propose that it originates from the reversal of velocity fluctuations required to maintain an average flow velocity at a site. The conjecture is motivated by a similar exponential decay (following transients) in the paradigmatic mean-reversing stochastic dynamics, the Ornstein-Uhlenbeck process [27]. Since mean reversal of velocity fluctuations is necessary to maintain the mean flow velocity at a location, it is a reasonable conjecture that the exponential decay of correlations will also hold for homogeneous flows, although experimental validation at small distances may be difficult. Figure 2(c) shows that the growth of the peak-width is linear both in the flow direction and normal to it. Although differences in the velocity of the correlation peak and the convection velocity have been reported in prior studies [13, 24, 28, 29], to the best of the authors' knowledge, this is the first quantitative assessment of the decay of the peak in inhomogeneous flows.

Figure2(e) shows an interesting observation. Due to the anisotropic growth rate and shape of the intense regions of $C(\mathbf{0}, \mathbf{R}'; \tau)$, the peak along any direction within a cone is seen to be approximately independent of the direction. The four lines are the peak locations as a function of time in directions bearing angles $\theta = 0$ (flow direction), $\theta = \tan^{-1}(1/6) = 9.46^o$, $\theta = \tan^{-1}(1/5) = 11.31^o$, and $\theta = \tan^{-1}(1/4) = 14.04^o$ to the flow direction, the lines being shifted for clarity. The slopes in all directions are nearly identical. (This direction-independence fails for smaller Reynolds numbers, see Figure 9 of Supplementary Materials.) However, as seen from Figure 2(d), the decay in the peak-intensity is not isotropic; it decreases faster as the deviation from the flow direction increases.

SPECTRAL ENERGY DENSITY

Velocity fluctuations in turbulent flows can be quantified via spectral components of the "energy field" $E(\mathbf{R}) = \frac{1}{2}\langle \mathbf{v}(\mathbf{R}, t) \cdot \mathbf{v}(\mathbf{R}, t) \rangle_t$ of a unit mass of fluid [4, 5]. When $E(\mathbf{R})$ is isotropic, dimensional considerations have been used to show that the spectral energy density scales as $\hat{E}(k) \sim k^{-5/3}$ in the inertial range [4, 5]. Due to lack of high resolution spatial data, most previous investigations used single-point velocity fluctuations and invoked

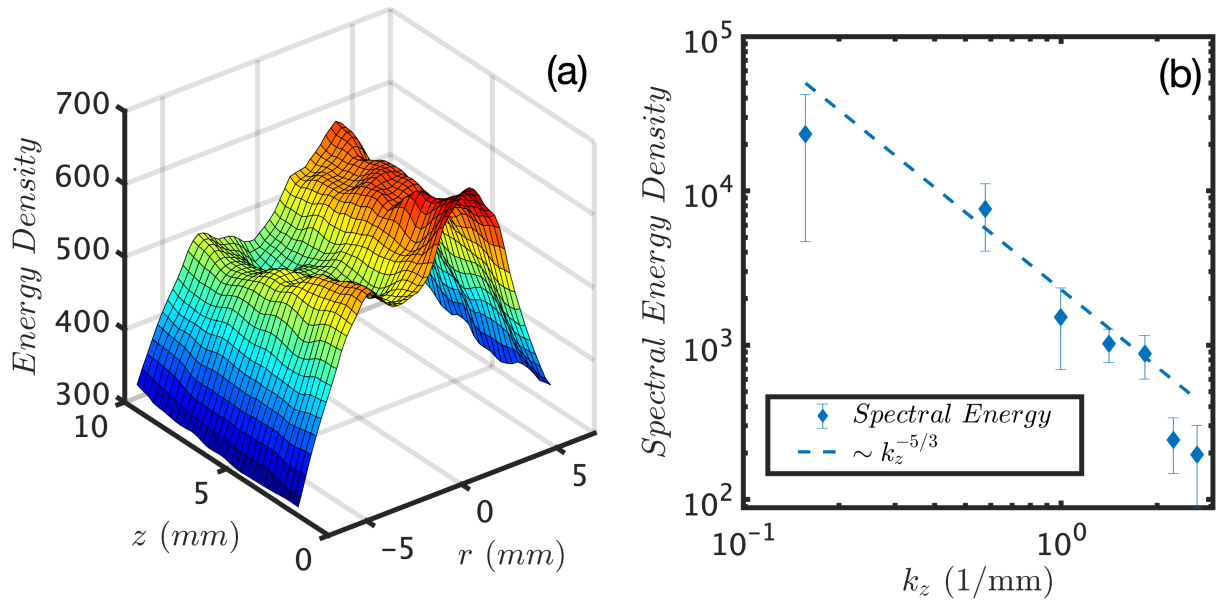

FIG. 3. (a) Energy density $E(r, z)$ for a jet-flow of $Re \approx 78,000$. (b) Decay of $\hat{E}(k_r = 0, k_z)$ as a function of k_z. Each diamond represents the mean of $\hat{E}(k_r = 0, k_z)$ at four successive points and error bars, the associated standard deviations. Dashed line shows Kolmogorov-Obukhov scaling.

Taylor's frozen hypothesis to establish the behavior of the Fourier spectrum $\hat{E}(\omega)$ of the time series [16, 30]. We wish to test for scaling of spectral energy in axisymmetric jet flow. Dimensional arguments analogous to those in Refs. [4, 5] show that the axial and radial components $\hat{E}_z$ and $\hat{E}_r$ of the spectral anergy will scale as $k_z^{-5/3}$ and $k_r^{-5/3}$ respectively.

The spatio-temporal velocity fields permit a direct computation of $E(\mathbf{R})$, which as seen from Figure 3(a), is not isotropic. Prior to computing the spectrum, we extend $E(\mathbf{R})$ in both the z and the r directions so that the extended field is periodic. The Fourier transform is performed on this extended field with periodic boundary conditions in order to minimize spurious spectral components. The z extension is a reflection across z_{max}. In the r direction, a linear transformation is applied on each z row of $E(\mathbf{R})$ so that the transformed field vanishes at the ends; it is then extended by reflection and multiplication by -1.

Since $E(\mathbf{R})$ for the jet flow is anisotropic, it is necessary to analyze the behavior of the 2-dimensional spectral energy density $\hat{E}(k_r, k_z)$. We find that $\hat{E}(k_r, k_z = 0)$ is several orders of magnitude smaller than $\hat{E}(k_r = 0, k_z)$. Figure 3(b) shows that the latter is consistent with the Kolmogorov-Obukhov [4, 5] law.

STRUCTURE FUNCTIONS

High-frequency, high-resolution velocity measurements aid in establishing several interesting statistical characterizations of point-wise and joint velocity-fluctuations in turbulent flows. The results from our analyses, presented in Supplementary Materials, can be summarized as follows: (a) Point-wise velocity fluctuations, both in the axial (v_z') and normal (v_r') directions, are nearly Gaussian distributed. Standard deviations in the axial and normal velocity fluctuations differ; specifically $\sigma(v_z') = 25.59 \pm 1.51\ m/s$ and $\sigma(v_r') = 17.80 \pm 0.51\ m/s$. Furthermore, $\sigma(v_z')$ exhibits a slow decay of $\sim 5\%$ over 17.7 mm in the down-flow direction. These observations imply the inhomogeneity and anisotropy of $\mathbf{v}'$. (b) As seen in Figure 4(d) of the Supplementary Materials, cross-correlation between point-wise axial and normal velocity fluctuations increases to the right and decreases to the left of the symmetry axis. This observation indicates that velocity fluctuations are not randomly oriented; the on-axis correlation is $\lesssim 0.1$. (Although the on-axis correlation should vanish by reflection symmetry, it is only approximately so for the < 0.1 sec. duration of the experimental signal.) (c) Distributions of pairwise velocity differences $\delta\mathbf{v}' \equiv \mathbf{v}'(\mathbf{R};t) - \mathbf{v}'(\mathbf{R}';t)$ are multivariate Gaussian when the two points are far apart, but develop broader tails as points are brought close to each other. In particular, they are nearly bi-exponential at the smallest distances [26, 31]. This anomaly may originate from incompressibility and the presence of tube-like vortex structures [22, 23]. Figure 2(a), provides an alternative interpretation: as the peak of the cross-correlation broadens, the strong correlation between velocity fluctuations at two neighboring sites with those at the origin at an earlier time implies the correlation of velocity fluctuations at the two points themselves.

Correlations between velocity fluctuations at neighboring sites can be characterized using the family of *structure functions*

$$S_\zeta\left(\mathbf{R},\mathbf{R}'\right) = \frac{\langle|(\mathbf{v}'(\mathbf{R};t) - \mathbf{v}'(\mathbf{R}';t))\cdot\mathbf{e}_\parallel|^\zeta\rangle_t}{\langle|\mathbf{v}'(\mathbf{R};t)\cdot\mathbf{e}_\parallel|^\zeta\rangle_t + \langle|\mathbf{v}'(\mathbf{R}';t)\cdot\mathbf{e}_\parallel|^\zeta\rangle_t}, \tag{2}$$

where $\mathbf{e}_\parallel \equiv \mathbf{e}_\parallel(\mathbf{R}' - \mathbf{R})$ is the unit vector in the direction $(\mathbf{R}' - \mathbf{R})$. Increasing ζ emphasizes larger deviations. We find that structure functions are homogeneous on the symmetry axis, *i.e.,* do not depend on the "origin" $\mathbf{R}$. Our computations of structure functions are implemented on a 60 ms (6000-frame) segment of the flow. The error bars in Figure 4

represent standard deviations for four different origins $\mathbf{R}$ on the symmetry axis.

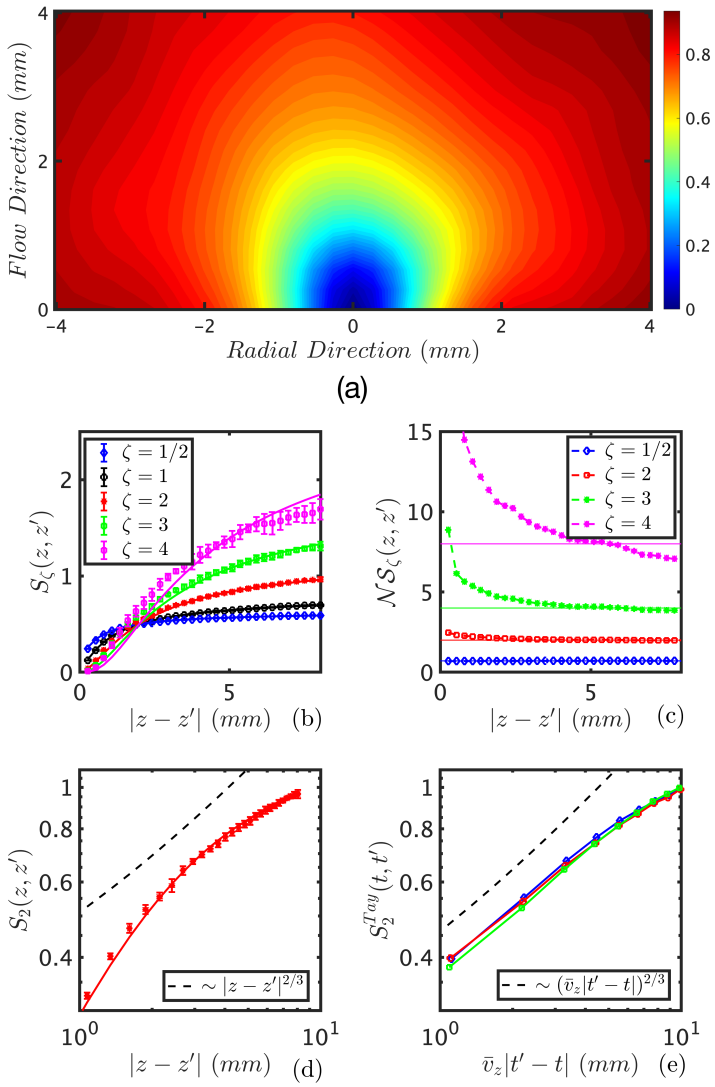

FIG. 4. (a) Contour plot for $S_1(\mathbf{R},\mathbf{R}')$ shows that it is nearly isotropic when $d = |\mathbf{R}'-\mathbf{R}|$ is small, but that the growth slows in the flow direction as d increases. (b) The symbols show values of the $S_{1/2}(\mathbf{R},\mathbf{R}')$, $S_1(\mathbf{R},\mathbf{R}')$, $S_2(\mathbf{R},\mathbf{R}')$, $S_3(\mathbf{R},\mathbf{R}')$, and $S_4(\mathbf{R},\mathbf{R}')$ in the flow direction, with error bars denoting standard deviations for four "origins" $\mathbf{R}$. The black line is the best fit of the data $S_1(z)$ for a functional form $S_1(z) = c_1 z^{c_3}/(1+c_2 z^{c_3})$ that satisfies the conditions for $|\mathbf{R}-\mathbf{R}'| \to 0$ and $|\mathbf{R}-\mathbf{R}'| \to \infty$. (c) The normalized structure functions $\mathcal{N}\mathcal{S}_\zeta(z)$ for $\zeta = 1/2,\ 2, 3,$ and 4, showing the validity of extended self-similarity [32, 33] for large $|z-z'|$. Extended self-similarity suggests that $S_\zeta(z) \approx 2^{\zeta-1} S_1(z)^\zeta$. These are the lines shown in (b). (d) $S_2(z,z')$ does not show an inertial range where the Kolmogorov $\frac{2}{3}$-law holds. (e) An assessment of the structure function from a single-point time series invoking Taylor's hypothesis is better approximated by the $\frac{2}{3}$-law.

Contour plot of $S_1(\mathbf{R},\mathbf{R}')$, Figure 4(a), shows that it is nearly isotropic when $|\mathbf{R}-\mathbf{R}'|$ is small, but that its growth slows in the flow direction with increasing $|\mathbf{R}-\mathbf{R}'|$. Additional

features of $S_\zeta(\mathbf{R},\mathbf{R}')$ can be inferred from observations on the distributions of velocity fluctuations outlined earlier. They include (a) continuity of velocity fluctuations imply that $S_\zeta(\mathbf{R},\mathbf{R}') \to 0$ as $|\mathbf{R}-\mathbf{R}'| \to 0$. (b) Since the distribution of velocity fluctuations at $\mathbf{R}$ and $\mathbf{R}'$ are multivariate normal and the $\mathbf{v}'$'s are independent when $|\mathbf{R}-\mathbf{R}'| \to \infty$, the distribution of $\mathbf{v}'(\mathbf{R};t) - \mathbf{v}'(\mathbf{R}';t)$ is multivariate normal with a variance-covariance matrix that is the sum of those for the two distributions. Since the variances of the distribution of axial velocity fluctuations are (nearly) constant within the entire domain, it is seen that $S_2(\mathbf{R},\mathbf{R}') \to 1$ as $|\mathbf{R}-\mathbf{R}'| \to \infty$. (c) In addition, $S_\zeta(\mathbf{R},\mathbf{R}') \to const.$ as $|\mathbf{R}-\mathbf{R}'| \to \infty$, the limiting value depending on ζ. Specifically, since $\mathbb{E}[|X|^\zeta] = \frac{2^{\zeta/2}}{\sqrt{\pi}}\,\Gamma\left(\frac{\zeta+1}{2}\right)\sigma^\zeta$ for a centered normal distribution of standard deviation σ, it can be shown that $S_\zeta(\mathbf{R},\mathbf{R}') \to 2^{\zeta/2-1}$ as $|\mathbf{R}-\mathbf{R}'| \to \infty$.

Figures 4(b) and (c) show the behavior of structure functions in the flow direction. Black diamonds in Figure 4(b) are the values of $S_1(z)$, with $z = |\mathbf{R}-\mathbf{R}'|$. Consistent with the limits for $z \to 0$ and $z \to \infty$, we use a 3-parameter fit $S_1(z) = c_1 z^{c_3}/(1+c_2 z^{c_3})$; the best fit is shown by the black line in Figure 4(b). The blue, red, green, and magenta symbols in Figure 4(b) represent $S_{1/2}(z)$, $S_2(z)$, $S_3(z)$, and $S_4(z)$ respectively. Next, given $S_\zeta(z) \to 2^{\zeta/2-1}$ when $z \to \infty$, we inquire if $S_\zeta(z)$ will be a power of $S_1(z)$. The conjecture is tested using the "normalized" structure function

$$\mathcal{NS}_\zeta(z) \equiv \frac{S_\zeta(z)}{S_1(z)^\zeta}. \tag{3}$$

The symbols in Figure 4(c), $\mathcal{NS}_{1/2}(z), \mathcal{NS}_2(z), \mathcal{NS}_3(z)$ and $\mathcal{NS}_4(z)$, illustrate that a power-relationship does hold for large z, the limiting value being consistent with $\mathcal{NS}_\zeta(z) = 2^{\zeta-1}$ (thin solid lines), except at the largest ζ. This is an example of *extended self-similarity* [32, 33]; it motivates us to inquire how well $S_\zeta(z)$ is approximated by $2^{\zeta-1}S_1(z)^\zeta$ in the entire range. The blue, red, green, and magenta lines in Figure 4(b) show that the approximation does hold over the entire domain, but weakens as ζ increases. It is shown in Supplementary Materials that (a) the discrepancy at large z can be attributed to small correlations and differences in point-wise standard deviations, and (b) the behavior for small z can be found using the near bi-exponential form of the distribution of velocity differentials.

The well-known Kolmogorov "$\frac{2}{3}$-law" states that for highly turbulent homogeneous and isotropic flows, there is an *inertial range*, terminating at the Taylor micro-scale, where

$S_2(\mathbf{R}, \mathbf{R}')$ is isotropic and scales like $|\mathbf{R}' - \mathbf{R}|^{2/3}$ [2, 3], and that higher-order structure functions scale as $S_\zeta(\mathbf{R}, \mathbf{R}') \sim |\mathbf{R}' - \mathbf{R}|^{\zeta/3}$. Experimental evidence for these claims, many of which are based on Taylor's frozen hypothesis, have not been conclusive. For example, while several studies appear to affirm isotropy of structure functions [34, 35], others report anisotropy [36, 37]. An inertial range is not observed in some studies on turbulent flows [31] and simulations [32], while it is found in others [9, 38, 39].

With high-resolution spatio-temporal flow fields, we are in a position to perform direct and indirect (*i.e.,* based on Taylor's frozen hypothesis) tests of Kolmogorov scaling in the anisotropic and inhomogeneous jet flow. Due to experimental noise and limitations on resolution, estimations of higher order moments are not reliable. The symbols in Figure 4(d) show $S_2(z, z')$ and the line through them the best fit to a functional form $S_2(z) = c_1 z^{c_3}/(1 + c_2 z^{c_3})$; the dashed line is the $\frac{2}{3}$-law. No inertial range is found for our data.

It has been conjectured that inhomogeneity and anisotropy induces deviations from a single scaling index [9], and that structure functions scale only within irreducible sectors of the $SO(3)$ symmetry group [10, 40–42]. The axisymmetric jet flows reported here show no scaling even within irreducible sectors.

Next, we inquire if use of Taylor's frozen hypothesis can contribute to experimental observations of an inertial range [9, 38, 39]. Under the scenario, single point velocity measurements at a location $\mathbf{R} = (0, z)$ on the symmetry axis can be used to evaluate the structure function in the flow-direction via

$$S_2^{Tay}(t, t') = \frac{\langle |v_z'(z;t) - v_z'(z;t'))|^2 \rangle_t}{2\langle |v_z'(z;t)|^2 \rangle_t}. \tag{4}$$

In Figure 4(e), we show the form of the structure function at three locations as a function of the *effective distance* $\bar{v}_z|t' - t|$, where $\bar{v}_z$ is the mean flow velocity at $\mathbf{R}$. Since the time interval between observations is 0.01 ms and the fluid speed in the flow direction is $\sim$ 130 m/s, the smallest effective distance accessible from the data is $\approx$ 1.3 mm; given that the Taylor micro-scale is ≈ 165 μm, we are unable to access the lower distances in the inertial scale. An inertial range cannot be observed, but $S_2^{Tay}(t, t')$ shows a closer agreement to the $\frac{2}{3}$-law than $S_2(\mathbf{R}, \mathbf{R}')$.

The primary motivation for our work was to highlight advantages of the acquisition of high-frequency, high-resolution spatio-temporal velocity fields in turbulent flows which, in

our case, was made through a long-duration (100-ms), high-energy burst-mode laser capable of producing pairs of pulses at a rate of up to 1 MHz [15]. As an example, we used the system to study turbulent jet flows at Reynolds numbers between 21,000 and 78,000, and showed that both the mean flow and velocity fluctuations are inhomogeneous and anisotropic. We inquired if and how Taylor's hypothesis is altered in the absence of isotropy and homogeneity. We found that the peak in the auto-correlation function flows at a rate that differs from the convection velocity and attributed it to non-uniformity of the mean flow. The peak correlation was found to decay exponentially in time. We argued that the observation can be attributed to mean-reversal of velocity fluctuations, which suggests that the decay will persist in homogeneous flows as well, even at short distances. Next we used the flow fields to test if scaling of structure functions [4, 5] and spectral energy density will continue to hold for inhomogeneous flows. Even though extended self-similarity [32, 33] holds except at small distances, we do not find an inertial range where the Kolmogorov $\frac{2}{3}$-law [3] holds. The decay of the axial component of the spectral energy density is consistent with the Kolmogorov-Obukhov law [4, 5].

METHODS

The N_2-jet, inserted through a cylindrical inlet of diameter 4.7 mm with a flow rate set by a mass flow controller (Alicat, MCR), expands axi-symmetrically into ambient stagnant air. The 2D velocity measurements are made on a grid inside the boundary of the expanding jet. Reynold's numbers at the inlet for our experiments range from 21,000 - 78,000 (see Supplementary Materials).

Velocity measurements are made using high-speed time-resolved PIV, whose acquisition rates in our system are limited primarily by repetition rates of laser sources and infrared camera memory. Wth an extended-duration dual-pulse burst-mode laser [16] we are able to acquire the flow field measurements at 100 kHz over a duration of 0.1 sec. The flow field was visualized using DEHS particles of diameter 0.25 μm. Under these conditions the motion of the particles is passive [16], and thus their flow will represent that of the fluid faithfully. The PIV resolution was made for each condition using the standard interpretation [20], requiring the vector correlation size (537 μm), laser sheet thickness (500 μm), and time resolution between correlated images (2 μs). For conditions analyzed, the spatial resolution

varies from 266 μm to 277 μm. Ref. [16] provides a detailed analysis of particle motion and rigorous definitions of spatial and temporal resolution. For all cases, a standard definition of resolution was used, *i.e.,* the Taylor micro-scale wave-vector at which the correction ratio of the squared spectral filtering function fell to 0.7. This can be interpreted as the point at which corrections of less than 30% are required to the spectral density tensor, in agreement with the standard work of Lavoie [20]. However, if a more stringent definition is applied (e.g. corrections less than 10%), then the effective spatial resolution would decrease.

The integral length scale was estimated as the product of the mean convective velocity and the measured integral time scale [43]. The time-scale was measured using the exponential decay of the temporal autocorrelation function [43]; the length-scale Λ was expressed in terms of the turbulence intensity (estimated from the standard deviation σ_1 in the axial direction) and the dissipation rate ε was estimated using $\Lambda \approx \sigma_1^3/\varepsilon$ [44]. The Taylor micro-scale was estimated by substituting this expression, yielding $\lambda \approx \sqrt{15\nu\Lambda/\sigma_1}$, and is a function of derived and measurable axial quantities in the experiment: kinematic viscosity ν, Λ, and σ_1. The Kolmogorov scale was estimated using the approximation $\eta \approx (\nu^3\Lambda/\sigma_1^3)^{1/4}$ [44]. Further details of these calculations can be found in Ref. [43].

The velocity measurements are made on a 67×51 grid placed symmetrically on an axial cross section, as illustrated schematically in Figure 1(a). There were a very few instances ($\sim 0.01\%$) where both the recorded axial *and* radial speeds vanish, indicating that the site was not seeded. (We find no cases where only one component vanishes.) Each such recording is replaced by the mean of the corresponding velocities at the same location in the time steps immediately preceding and following the instance.

Acknowledgements: This research was supported by the Air Force Research Laboratory under Contract No. FA8650-15-D-2518. This manuscript is approved for public release by the Air Force Research Laboratory (88ABW-2020-1243).

---

[1] Reynolds, O. On the dynamical theory of incompressible viscous fluids and the determination of the criterion. *Philosophical Transactions of the Royal Society of London* **186**, 123–161 (1894).

[2] Monin, A. S. & Yaglom, A. M. *Statistical Fluid Mechanics, Mechanics of Turbulence, Vol. I*

(Dover Publications, Inc., New York, 1971).

[3] Kolmogorov, A. N. Local structure of turbulence in an incompressible fluid at very high Reynolds numbers. *Dokl. Akad. Naud. SSSR* **30**, 299–303 (1941).

[4] Kolmogorov, A. N. Energy dissipation in locally isotropic turbulence. *Dokl. Akad. Naud. SSSR* **32**, 19–21 (1941).

[5] Obukhov, A. M. Energy distribution in the spectrum of a turbulent flow. *Izvestiya Akad. Nauk. SSSR, Ser. Geogr. Geofiz.* **4-5**, 453–466 (1941).

[6] Richardson, L. F. *Weather prediction by numerical processes* (Cambridge University Press, Cambridge, 1922).

[7] Taylor, G. I. The spectrum of turbulence. *Proc. R. Soc. London, Ser. A* **164**, 476 (1938).

[8] Saddoughi, S. G. and Veeravalli, S. V. Local isotropy in turbulent boundary layers at high Reynold's number. *Journal of Fluid Mechanics* **268**, 333–372 (1894).

[9] Anselmet, F. and Gagne, Y. and Hopfinger, E. J. and Antonia, R. High-order velocity structure functions in turbulent shear flows. *Journal of Fluid Mechanics* **140**, 63–89 (1984).

[10] Biferale, L. and Procaccia, I. Anisotropy in turbulent flows and in turbulent transport. *Physics Reports* **414**, 43–164 (2005).

[11] Procaccia, I. and Sreenivasan, K. R. The state of the art in hydrodynamic turbulence: Past successes and future challenges. *Physica D-Nonlinear Phenomena* **237**, 2167–2183 (2008).

[12] Sreenivasan, K. R. and Druva, B. Is there scaling in high-Reynolds-number turbulence? *Progress in Theoretical Physics, Supplement* **130**, 103–120 (1998).

[13] Lv́ov, V. S. and Pomyalov, A. and Procaccia, I. Temporal surrogates of spatio-temporal turbulent statistics: the Taylor hypothesis revisited. *Physical Review E* **60**, 4175–4184 (1999).

[14] Belmonte, A. and Martin, B. and Goldburg, W. I. Experimental study of Taylor's hypothesis in a turbulent soap film. *Physics of Fluids* **12**, 835–845 (2000).

[15] Slipchenko, M. and Miller, J. D. and Roy, s. and Meyer, T. R. and Mance, J. G. and Gord, J. R. 100-kHz, 100-ms, 400-J Burst-Mode Laser with Dual-Wavelength Diode-Pumped Amplifiers. *Optics Letters* **39**, 4735–4738 (2014).

[16] Miller, J. D. and Jiang, N. and Slipchenko, M. N. Mance, J. G. Meyer, T. R. and Roy, S. and Gord, J. R. Spatiotemporal analysis of turbulent jets enabled by 100-kHz, 100-ms burst-mode particle image velocimetry. *Exp. Fluids* **57**, 192 (2016).

[17] Tollmien, W. Berechnung turbulenter ausbreitungsvorgänge. *Zs. angew. Math. Mech.* **6**,

468–478 (1926).

[18] Rajaratnam, N. *Turbulent Jets* (Elsevier Scientific Publishing Company, Amsterdam, 1976).

[19] Frisch, U. *Turbulence: The Legacy of A. N. Kolmogorov* (Cambridge University Press, Cambridge, 1995).

[20] Lavoie, P. and Avallone, G. and De Gregorio, F. and Romano, G. P. and Antonia, R. A. Spatial resolution of PIV for the measurement of turbulence. *Exp.Fluids* **43**, 39–51 (2007).

[21] Hua, J.-C. and Gunaratne, G. H. and Talley, D. G. and Gord, J. R. and Roy, S. Dynamic-mode decomposition based analysis of shear coaxial jets with and without transverse acoustic driving. *Journal of Fluid Mechanics* **790**, 5–32 (2016).

[22] Siggia, E. Numerical study of small-scale intermittency in 3-dimensional turbulence. *Journal of Fluid Mechanics* **107**, 375–406 (1981).

[23] She, Z. S. and Jackson, E. and Orzag, S. Intermittent vortex structures in homogeneous isotropic turbulence. *Nature* **344**, 226–228 (1990).

[24] Zaman, K. B. M. Q. and Hussain, A. K. M. F. Taylor hypothesis and large-scale coherent structures. *Journal of Fluid Mechanics* **112**, 379–396 (1981).

[25] Koeltzsch, K. On the relationship between Lagrangian and Eulerian time scale. *Atmospheric Environment* **33**, 117–128 (2005).

[26] Burghelea, T. and Segre, E. and Steinberg, V. Validity of the Taylor hypothesis in a random spatially smooth flow. *Physics of Fluids* **17**, 103101 (2005).

[27] Uhlenbeck, G. E. and Ornstein, L. S. On the theory of Brownian motion. *Physical Review* **36**, 823–841 (1930).

[28] Dahm, W. J. A. and Southerland, K. B. Experimental assessment of Taylor's hypothesis and its applications to dissipation estimates in turbulent flows. *Physics of Fluids* **9**, 2101–2117 (1997).

[29] Mesbah-Uddin, A. K. and Perry, A. E. and Marusic, I. On the validity of Taylor's hypothesis in wall turbulence. *Journal of Mechanical Engineering Research and Development* **19-20**, 57–66 (1997).

[30] Tabeling, P., Zocchi, G., Belin, F., Maurer, J. & Willaime, H. Probability density functions, skewness, and flatness in large reynold's number turbulence. *Physical Review E* **53**, 1613–1621 (1996).

[31] Lewis, G. S. and Swinney, H. L. Velocity structure functions, scaling, and transitions in

high-Reynolds-number Couette-Taylor flow. *Physical Review E* **59**, 5457–5467 (1999).

[32] Benzi, R. and Ciliberto, S. and Tripiccione, R. and Baudet, C. and Massaioli, F. and Succi, S. Extended self-similarity in turbulent flows. *Physical Review E* **48**, R29–R32 (1993).

[33] Ciliberto, S. Extended self-similarity. In *Turbulence*, 27–30 (NATO ASI Series (Series B: Physics), Vol. 341, 1995).

[34] Cammusi, R. and Barbagallo, D. and Guj, R. and Stella, F. Transverse and longitudinal scaling laws in non-homogeneous low Re turbulence. *Physics of Fluids* **8**, 1181–1191 (1996).

[35] Noullez, A and Wallace, G and Lempert, W. and Miles, R. B. and Frisch, U. Transverse velocity measurements in turbulent flows using RELIEF technique. *Physics of Fluid Mechanics* **339**, 287–307 (1997).

[36] Cammusi, R. and Benzi, R. Hierarchy of transverse structure functions. *Physics of Fluids* **9**, 257–259 (1997).

[37] Chen, S. and Sreenivasan, K. and Nelkin, M. and Cao, N. Z. Refined similarity hypothesis for transverse structure functions in fluid turbulence. *Physical Review Letters* **79**, 2253–2256 (1997).

[38] Arneodo, A., Baudet, F., Belin, F. & et al. Structure functions in turbulence in various flow configurations at Reynolds numbers between 30 and 5000. *Europhysics Letters* **34**, 411–416 (1996).

[39] Saw, E.-W. and Debue, P. and Kuzzay, D. and Daviaud, F. and Dubrulle, B. On the universality of anomalous scaling exponents of structure functions in turbulent flows. *Journal of Fluid Mechanics* **837**, 657–669 (2018).

[40] Arad, I. and L'vov, V. S. and Procaccia, I. Anomalous scaling in anisotropic turbulence. *Physica A* **288**, 280–307 (2000).

[41] Kurien, S. and L'vov, V. S. and Procaccia, I. and Sreenivasan, K. R. Scaling structure of the velocity statistics in atmospheric boundary layers. *Physical Review E* **61**, 407–421 (2000).

[42] Kurien, S. and Sreenivasan, K. R. Anisotropic scaling contributions to high-order structure functions in high-Reynolds-number turbulence. *Physical Review E* **62**, 2206–2212 (2000).

[43] Miller, J. D. and Gord, J. R. and Meyer, T. R. and Jiang, N. and Thule, D. and Slipchenko, M. N. and Mance, J. G. and Roy, S. 100 kHz burst-mode particle image velocimetry: space-time correlations and considerations for spatial and temporal resolution. In *Turbulence*, 1–12 (54th AIAA Aerospace Sciences Meeting, Jan. 4-8 2016, San Diego, CA, 2016).

[44] Pope, S. B. *Turbulent Flows* (Cambridge University Press, Cambridge, UK, 2000).

Figures

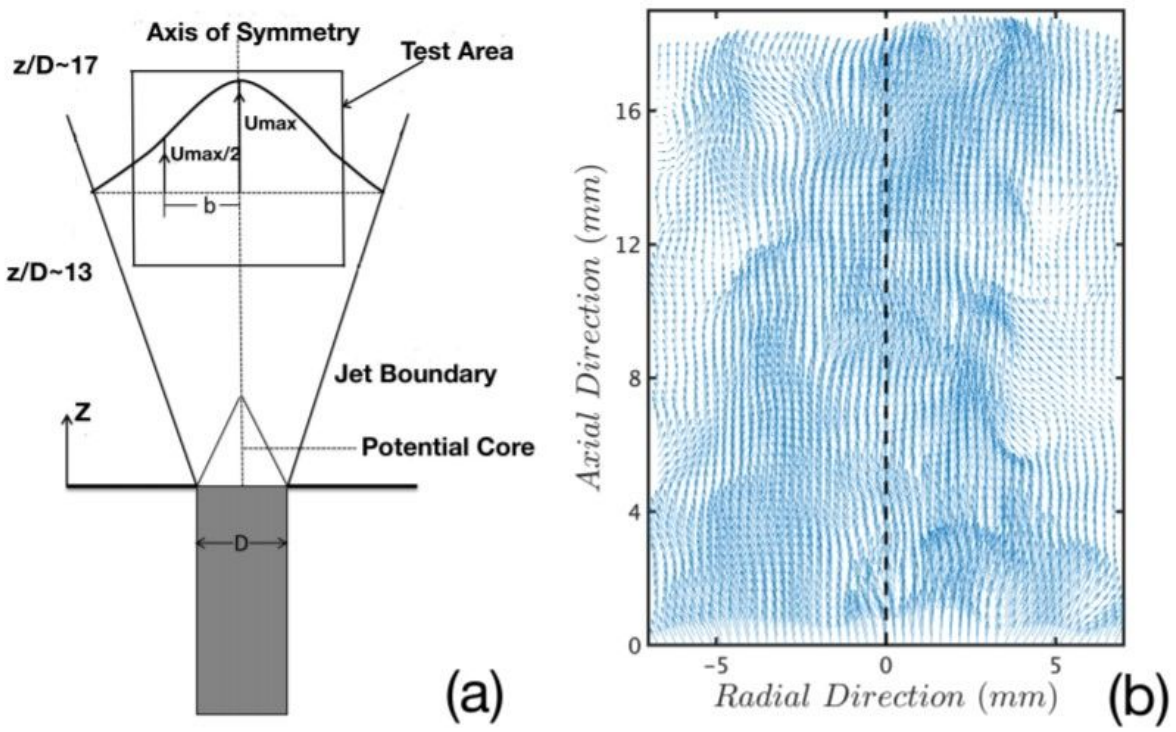

Figure 1

(a) Axisymmetric jet flow is generated by N2 gas ejected from cylinder of radius D = 4.7 mm. Rectangular region of size 13.4 mm × 17.7 mm where velocity measurements were made was approximately 13D downstream of inlet. (b) Snapshot of velocity field for flow of Re ≈ 78, 000.

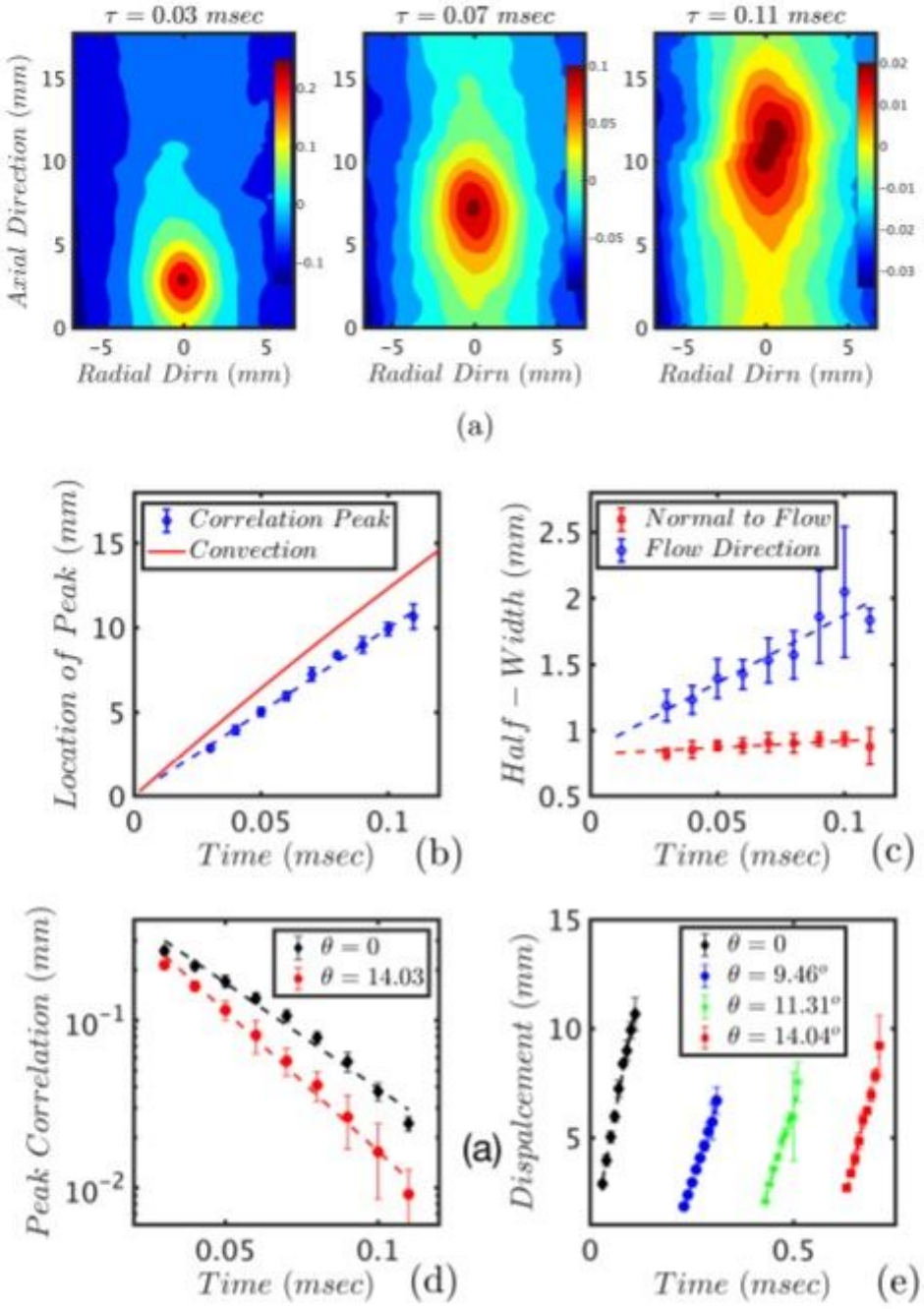

Figure 2

(a) Three snapshots of the field C (R = 0, R0 ; τ), whose peak flows downstream and broadens in time. Distances are given in mm and the center of the near-boundary is chosen as the origin. (b) The downstream velocity of the peak is smaller than the convection velocity. (c) The width of the peak, both in the flow direction and normal to it, grows linearly in time. (d) The peak Pz(τ) (flow direction: θ = 0) decays exponentially in time. (e) Velocity of the peak is nearly independent of the direction inside of a cone. The lines (shifted for clarity) show the peak locations as a function of time for the flow direction

and for directions oriented θ = tan−1 (1/6), tan−1 (1/5), and tan−1 (1/4) from the flow axis. However, as seen in (d), the peak intensity decays faster as one moves away from the flow direction.

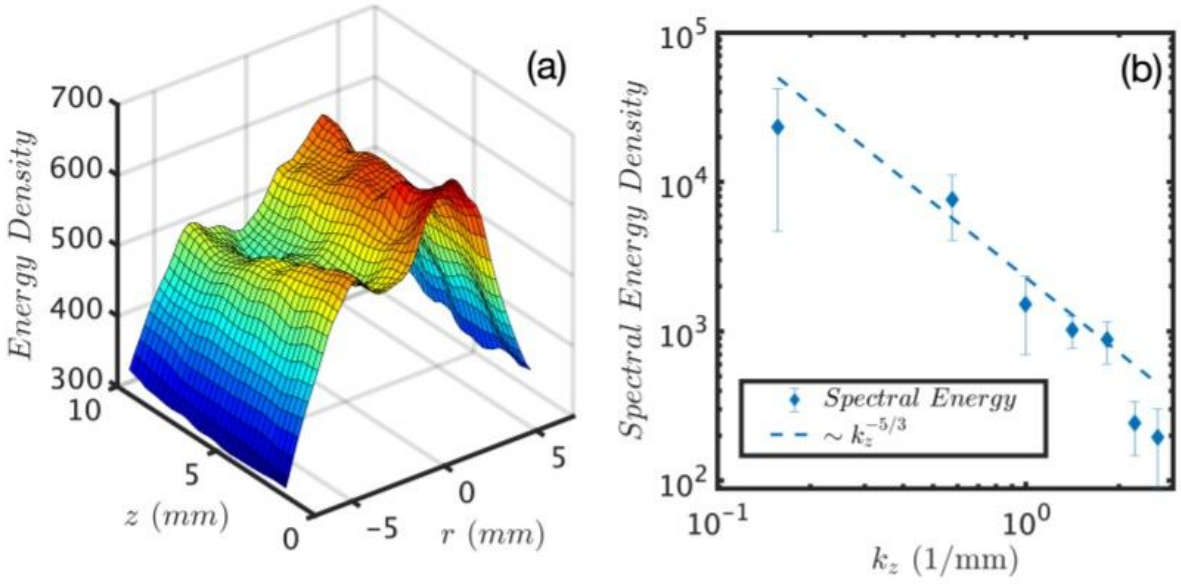

Figure 3

(a) Energy density E(r, z) for a jet-flow of Re ≈ 78, 000. (b) Decay of Eˆ(kr = 0, kz) as a function of kz. Each diamond represents the mean of Eˆ(kr = 0, kz) at four successive points and error bars, the associated standard deviations. Dashed line shows Kolmogorov-Obukhov scaling.

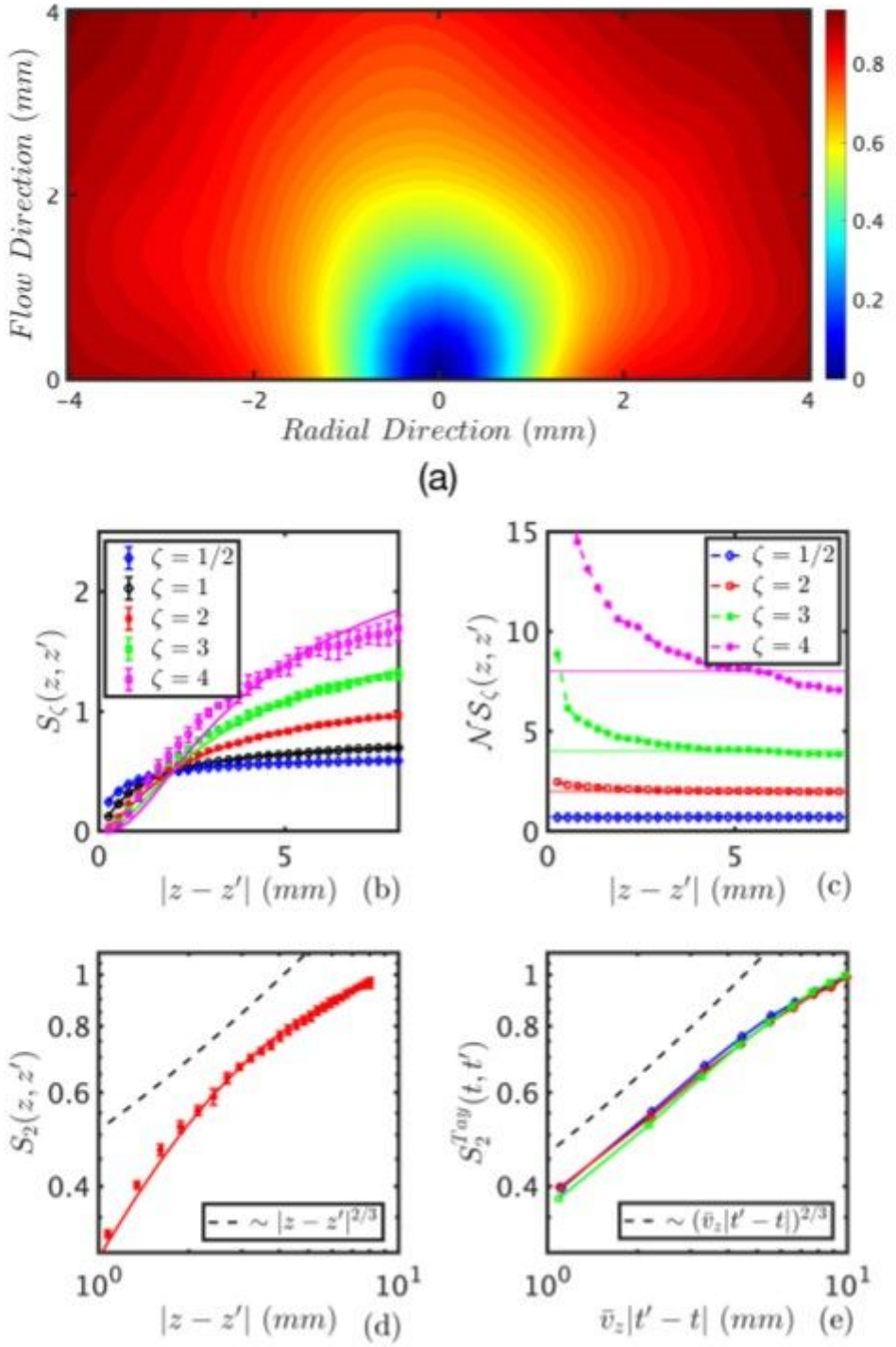

Figure 4

(a) Contour plot for S1 (R, R0) shows that it is nearly isotropic when d = |R0 −R| is small, but that the growth slows in the flow direction as d increases. (b) The symbols show values of the S1/2 (R, R0), S1 (R, R0), S2 (R, R0), S3 (R, R0), and S4 (R, R0) in the flow direction, with error bars denoting standard deviations for four “origins” R. The black line is the best fit of the data S1(z) for a functional form S1(z) = c1z c3 /(1 + c2z c3) that satisfies the conditions for |R − R0 | ⍰ 0 and |R − R0 | ⍰ ∞. (c) The normalized structure functions N Sζ (z) for ζ = 1/2, 2, 3, and 4, showing the validity of extended self-similarity [32, 33]

for large |z − z 0 |. Extended self-similarity suggests that Sζ (z) ≈ 2 ζ−1S1(z) ζ . These are the lines shown in (b). (d) S2(z, z0) does not show an inertial range where the Kolmogorov 2 3 -law holds. (e) An assessment of the structure function from a single-point time series invoking Taylor's hypothesis is better approximated by the 2 3 -law.

Supplementary Files

This is a list of supplementary files associated with this preprint. Click to download.

- SupplementaryMaterials.pdf